Smart electrochemical immunosensing of aflatoxin B1 based on a palladium nanoparticle-boron nitride-coated carbon felt electrode for the wine industry

Kwanele Kunene, Syreina Sayegh, Matthieu Weber, Myalowenkosi Sabela, Damien Voiry, Igor Iatsunskyi, Emerson Coy, Suvardhan Kanchi, Krishna Bisetty, Mikhael Bechelany

Smart Electrochemical Immunosensing of Aflatoxin B_1 Based on a Palladium Nanoparticle-Boron Nitride-Coated Carbon Felt Electrode for the Wine Industry

Kwanele Kunene[a,b], Syreina Sayegh[a], Matthieu Weber[a], Myalowenkosi Sabela[b], Damien Voiry[a], Igor Iatsunskyi[d], Emerson Coy[d], Suvardhan Kanchi[b,c], Krishna Bisetty[b*], Mikhael Bechelany[a*]

[a]*Institut Européen des Membranes, IEM, UMR 5635, Univ Montpellier, CNRS, ENSCM, Montpellier, France*

[b]*Department of Chemistry, Durban University of Technology, P.O. Box 1334, Durban 4000, South Africa*

[c]*Department of Chemistry, Sambhram Insitute of Technology, via Jalahalli East, M.S. Palya, Bengaluru 560097, India.*

[d]*NanoBioMedical Centre, Adam Mickiewicz University in Poznan, 3 Wszechnicy Piastowskiej str., 61-614, Poznan, Poland*

Abstract

This study describes the fabrication of an aflatoxin (AFB_1) electrochemical immunosensor by immobilization of an anti-AFB_1 antibody-bovine serum albumin (BSA) conjugate on a layer of L-cysteine (L-Cys) used to link the antibody to the palladium nanoparticle-boron nitride (PdNP-BN)-modified carbon felt (CF) electrode. Each step of the immunosensor fabrication was characterized using cyclic voltammetry (CV) and electrochemical impedance spectroscopy (EIS). These two analyses demonstrated that BN acted as a substrate for PdNPs and also as an electroactive material that enhanced the immunosensor electrical conductivity. Different features (antibody concentration, pH, incubation time) were optimized to enhance the immunosensor analytical performance. In these conditions, the fabricated immunosensor displayed a large linear range (1-10 ng mL^{-1}; R^2 = 0.9987), low limit of detection (0.834 ng mL^{-1} AFB_1), and was stable for up to 3 weeks. The fabricated electrochemical immunosensor could detect AFB_1 in wine samples with recovery levels of 93-106%. Lastly, the Monte Carlo simulation studies confirmed the stronger binding of the anti-AFB_1 antibody-BSA conjugate to the L-Cys/PdNP-BN/CF electrode surface, and molecular docking confirmed the docking of BSA subdomain II to the anti-AFB_1 antibody.

Keywords: Aflatoxin B_1; wine sample; Atomic Layer Deposition, palladium nanoparticles; boron nitride; immunosensor

[†]Corresponding author(s) Email.: mikhael.bechelany@umontpellier.fr (M. Bechelany), bisettyk@dut.ac.za (K. Bisetty)

1. Introduction

Wine is one of the most important alcoholic beverages in many societies. Besides its very well-known adverse effects, wine may also contain various toxins and contaminants because grapes can be contaminated by very harmful mycotoxins, such as aflatoxins [1]. Therefore, their presence in wine must be monitored to ensure the product safety. Aflatoxins are highly toxic substances produced by some molds, such as *Aspergillus flavus* and *Aspergillus parasiticus* [2-4]. There are different aflatoxin types (AFB_1, AFB_2, AFG_1 and AFG_2) as well as two aflatoxin metabolites (AFM_1 and AFM_2) [5]. AFB_1 is the most toxic, mutagenic, teratogenic, and carcinogenic aflatoxin [6, 7]. According to the International Agency for Research on Cancer (IARC), AFB_1 is a group 1 carcinogen [8, 9]. AFB_1 has been detected in many different food products, such as wine, grape juice, rice, pasteurized milk, and maize [2, 3, 6, 10-12]. The maximum permissible AFB_1 level in food samples differs among countries. For instance, this level is 5 μg/kg in South Korea and 2 μg/kg in the European Union [13]. Therefore, AFB_1 must be quantified to avoid the supply and ingestion of contaminated food products.

AFB_1 can be detected using analytical methods (e.g. liquid chromatography-mass spectrometry [14], enzyme-linked immunosorbent assay [15], thin-layer chromatography [16], high-performance liquid chromatography [17]) and optical methods [18, 19]. These techniques are sensitive and specific, but they are laborious and require well-trained operators, extensive sample pre-treatment, and expensive instruments. Thus, rapid, sensitive, selective and cheaper techniques to precisely quantify AFB_1 levels in foods and beverages are urgently needed to be used by industries and inspection agencies. In the last few decades, a significant number of electrochemical sensing methods have been proposed for AFB_1 detection: electrochemical sensors [20], electrochemiluminescence [21], photoelectrochemical sensors [22], and electrochemical immunosensors [23]. Electrochemical immunosensors display very good sensitivity, efficiency, specificity, and consistency. They are also cheap and easy to use. The

goal of the present study was to design and fabricate smart 2D materials to improve sensing platforms for AFB_1 detection in wine samples.

When designing electrochemical immunosensors, electrode modification is a well-known procedure for modifying the electrical conductivity and specific surface area to increase the immunosensor sensitivity. Recently, many studies have focused on palladium nanoparticles (PdNPs) due to their conductive features, large surface area, catalytic, and electronic properties [24, 25]. Furthermore, PdNPs have become a common material in the biosensing field [26, 27]. Previous studies have shown that the nanoparticle (NP) size should be reduced to improve the catalytic activity. The NP supporting material also plays a crucial role [28, 29]. Carbon and high melting point oxides are frequently used as supporting material, but boron nitride (BN)-based materials are a new interesting alternative [30-32]. Indeed, BN is a promising supporting substrate for electrochemical sensors due to its remarkable features, such as high surface area, low toxicity, and good catalytic properties [33, 34]. Moreover, the growth of metal NPs on the BN support can improve the sensing of different analytes [35]. Therefore, using BN as substrate for PdNP deposition appears to be a promising route for electrochemical sensor development. There are several methods for growing NPs on the BN support: electrodeposition [36], hydrothermal deposition [37], chemical vapour deposition [38], spray drying and pyrolysis [39]. They require high temperatures, toxic precursors, and complex and long experimental methods. For this reason, atomic layer deposition (ALD) is now considered the most effective method for BN and PdNP synthesis with excellent uniformity [29]. It also provides NPs and films with high conformality aspect ratio and controlled thickness [40]. Therefore, for many applications, such as biosensors, thin films and membranes, ALD is an effective method for depositing films and NPs [40-42].

Besides the substrate material, the method used to fabricate the electrochemical immunosensor also strongly contributes to enhance its analytical performance.

L-cysteine (L-Cys) is an amino acid that contains an amino, sulfhydryl and carboxylic functional group. L-Cys has distinctive properties and is extensively used in biological, environmental and electrochemical research [43-45]. Furthermore, L-Cys has been used for providing a self-assembly layer and for changing the surface of noble metal NPs [46, 47]. L-Cys harbours different functional groups, such as the -SH groups that binds to the NP surface, and the (COOH) and (-NH_2) groups that stabilize NPs [48] and offer a hydrophilic interface for the analyte-NP surface interaction [49, 50].

In a previous study, we described the synthesis of PdNPs on carbon felt (CF) using ALD for bio-sensing applications [51]. Specifically, we developed an electrochemical immunosensor for AFB_1 detection by growing PdNPs on a thin layer of BN, using L-Cys for palladium-sulphur bond (Pd-S bonds) formation for the anti-AFB_1 antibody attachment.

The current study focused on the fabrication of an electrochemical immunosensor for AFB_1 detection in wine samples using L-Cys/PdNP-BN followed, for the first time, by computational modelling of the anti-AFB_1 antibody binding to the L-Cys/PdNP-BN/CF electrode surface. Our study revealed that the fabricated immunosensor is a proficient tool for the detection of AFB_1 in wine samples.

2. Experimental

2.1. Materials and reagents

CF MGL 190, fuel cell earth (10 Draper St. Unit 32 Woburn, MA, MA 01801 www. Fuelearth.com), ammonia (NH_3) (Air Liquide Paris, France), L-Cys (99.0% purity), *N*-hydroxysuccinimide (NHS; 98.0% purity), *N*-ethyl-N-(3-dimethylaminopropyl carbodiimide (EDC; 97.0% purity), AFB_1 (3.79 µg g^{-1} in acetonitrile), ochratoxin A (OTA; 1 mg mL^{-1} in DMSO, 98.0% purity), ethanol (CH_3CH_2OH; 95.0% purity), potassium ferricyanide ($[(Fe(CN)_6]^{3-}$, 99.0% purity), potassium ferrocyanide ($[(Fe(CN)_6]^{4-}$, 98.5-102.0% purity),

acetonitrile (CH_3CN; 99.8% purity), boron tribromide (BBr_3; 99.9% purity), dipotassium hydrogen phosphate (K_2HPO_4; 98.0% purity), potassium dihydrogen phosphate (KH_2PO_4; 99.0% purity), sulphuric acid (H_2SO_4; 95.0-98.0% purity), formaldehyde solution (CH_2O; ACS reagent, 37 wt. % in H_2O, with 10-15% of methanol as stabilizer), bovine serum albumin (BSA; 98.0% purity), palladium (II) hexafluoroacetylacetonate [($Pd(C_5HF_6O_2)_2$, 99.0% purity], and rabbit anti-AFB_1 polyclonal antibodies were purchased from Sigma Aldrich France. Ultrapure water (Mill-Q, Millipore, 18.2 MΩ resistivity) was used for all experiments.

2.2.Apparatus and characterization

The measurements using linear sweep voltammetry (LSV) and cyclic voltammetry (CV) were performed on the Solartron 1286 electrochemical interface (TICS International Ltd., UK), using a three-electrode system: working electrode (modified CF: 3.5 cm x 0.7 cm x 0.3 cm in size), auxiliary electrode (graphite rod), and reference electrode (Ag/AgCl). An iS50 ATR Thermo Scientific spectrophotometer (range: 400-4000 cm^{-1}) was used to acquire attenuated total reflectance (ATR) spectra. The SP-150 EC-LAB Electrochemistry chemical workstation (VSP Potentiostat from BioLogic Science Instruments, France) was used for electrochemical impedance spectroscopy (EIS) analyses carried out at ~25.0 °C. The fabricated immunosensor was morphologically characterized using an atomic force microscope (AFM, Veeco Nanoscope Dimension 3100). A VG ESCALAB 250 spectrometer (Thermo Fisher Scientific, Waltham, MA, USA) was used for X-ray photoelectron spectroscopy (XPS), and a JEOL ARM 200F high-resolution transmission electron microscope (200 kV) with an EDX analyser (JED2300, at least 30 accumulations, matrix 512 × 512 points in STEM mode) for the high-resolution transmission electron microscopy (HR-TEM) analysis.

2.3. Antibody and sample preparation

The 0.1M phosphate buffer saline (PBS) solution (pH 7.5) was prepared by mixing an equimolar ratio of dipotassium hydrogen phosphate and potassium dihydrogen phosphate. This PBS solution was used to dilute the anti-AFB_1 antibody (1 µg mL^{-1}). AFB_1 was dissolved in PBS with 10% methanol and stored at 20 °C. A BSA solution (1 µg mL^{-1} in PBS) was used as blocking agent.

The red wine samples were prepared following the procedure described by Goud and co-workers [9]. Wine was mixed with PBS and acetonitrile (1:3:1). The mixture was then sonicated for 1h, centrifuged at 5000 rpm for 1h, and filtered using a micro-filter with pore size 0.1-10 µm. The filtrate was spiked with different concentrations of AFB_1 and used for recovery studies with the fabricated immunosensor.

2.4. CF pre-treatment

CF were pre-treated to change their hydrophobic nature to hydrophilic using the method described by Kosimaningrum and co-workers [52]. To eliminate the impurities that might be present on the surface, CF were ultra-sonicated in ethanol for 2h, washed with deionized distilled water, and oven-dried at 70 °C overnight. Then, CF were electrochemically pre-treated in 1M H_2SO_4 by CV from 0 to 1.5 V versus Ag/AgCl for 30 cycles at 20 mV s^{-1}. Finally, samples were thoroughly washed with deionized distilled water until neutral pH and oven-dried at 70 °C.

2.5. Synthesis of PdNPs on BN by ALD

A homemade low-pressure ALD reactor was used to deposit BN and PdNPs onto the CF surface. BN deposition was carried out at 750 °C, using BBr_3 and NH_3 as precursor and co-reactant, respectively [53]. The process consisted in: BBr_3 pulse for 0.1s, exposure for 5s, purge

with inert gas for 15s, NH_3 pulse for 3s exposure to gas for 5s, and purge for 15s. The obtained samples are called BN/CF hereafter.

For PdNP deposition on BN/CF (PdNP-BN/CF hereafter), the hot-wall chamber temperature was maintained at 220 °C, while $Pd(C_5HF_6O_2)_2$ was heated to 70 °C in a sealed stainless steel bottle to reach a sufficiently high vapor pressure. The inlet lines were heated to 100 °C to limit condensation. PdNPs (200 cycles) were deposited on BN/CF following the procedure recently described by our team [51]. One Pd cycle was completed by first dosing $Pd(C_5HF_6O_2)_2$, followed by exposure for 15s and purge with argon gas for 10s. Then, formalin was pulsed for 1s, followed by exposure for 15s, and a final purge for 60s.

2.6. Fabrication of the label-free BSA/anti-AFB_1/L-Cys/PdNP-BN/CF immunosensor

Fig. 1 summarizes the fabrication process of the electrochemical immunosensor for AFB_1 detection in wine samples. First, the PdNP-BN/CF electrode was immersed in a 10 $mmoL^{-1}$ L-Cys solution at room temperature overnight to form Cys/NP thiolate bonds. After washing with PBS to remove unbound L-Cys molecules, 20 µL of 0.4 mol L^{-1} EDC and 0.1 mol L^{-1} NHS (1:3 ratio) were dropped on the L-Cys/PdNP-BN/CF electrode at room temperature for 50 min to convert the terminal carboxylic groups to active NHS esters [54]. Then, the modified electrode was rinsed with PBS, and 20 µL of anti-AFB_1 antibody solution (1.0 µg mL^{-1} in PBS) was spread over the L-Cys/PdNP-BN/CF electrode surface and incubated at 4.0 °C for 2h. The resulting anti-AFB_1/L-Cys/PdNP-BN/CF electrode was rinsed with PBS to remove the excess antibody. Then, to block the non-active sites, 10 µL of BSA (10%, m/v) was dropped on the anti-AFB_1/L-Cys/PdNP-BN/CF electrode and left at room temperature for 20 min (BSA/anti-AFB_1/L-Cys/PdNP-BN/CF). When not used, electrodes were stored at 4 °C.

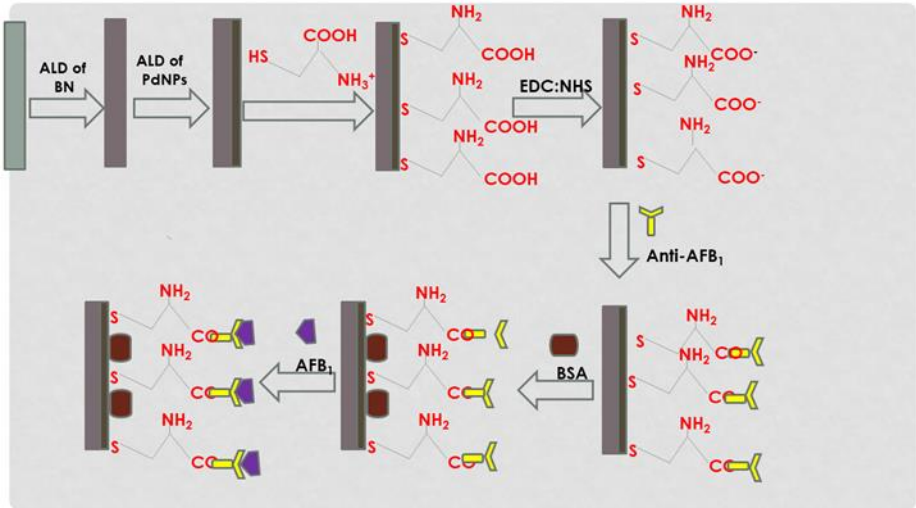

Fig. 1: Schematic representation of the fabrication procedure of an electrochemical immunosensor for AFB_1 detection in wine samples.

2.7. Biorecognition experiments

The biorecognition experiments were carried out by dipping the BSA/anti-AFB_1/L-Cys/PdNP-BN/CF electrode in a cell that contained 20 mL PBS (pH 7.5). Then, 10 µL of AFB_1 solution at different concentrations (1.0, 2.0, 4.0, 6.0, 8.0 and 10 ng mL^{-1}) was added to the cell for 30 min. Similar experiments were performed using wine samples that contained different AFB_1 concentrations. All experiments were done three times.

2.8. Safety considerations

As AFB_1 is a potent carcinogen, protective gloves, safety goggles, and disposable face mask were used during the experiments. The contaminated glassware was soaked in a sodium hypochlorite solution (5.25%) for 72h before washing.

3. Computational modelling

3.1. Molecular docking of the anti-AFB_1 antibody with BSA (BSA-anti-AFB_1)

The 3D structure of the monoclonal antibody against AFB_1 was obtained from the RCSB Protein Data Bank (1IGY). This entry contains four unique chains (A-D) and 12750 atoms, including 2498 hydrogen atoms and 0 deuterium atoms [55]. The crystal structure of BSA (RCSB Protein Data Bank; 3v03) contained two unique chains (A and B) and 8828 atoms (0 hydrogen and 0 deuterium) [56]. The antibody was docked to BSA using the ClusPro protein-protein docking server, with advanced options set to antibody mode [57], and the results were visualized using Discovery Studio Visualizer.

3.2. Nanocluster construction

The CF, BN and Pd nanoclusters were built using the Build option and the standard library of parameters of the BIOVIA Materials Studio software package [58]. The 3D nanoclusters were energy-minimized and their geometry optimized with the Forcite module and the UNIVERSAL force field.

3.3. Monte Carlo simulations of the BSA/anti-AFB_1/L-Cys/PdNP-BN/CF electrode adsorption capacity

Monte Carlo simulations were used to determine the lowest energy configurations of the L-Cys/PdNPs-BN/CF electrode (the adsorbate) on the BSA-anti-AFB_1 surface (the substrate) at progressively decreasing temperatures. The Adsorption Locator module in the Material Studio package (as preparatory and screening tool) and the force-field method were used to rank the obtained energy configurations, and to identify the preferred adsorption sites. Monte Carlo simulations of the adsorbate-substrate configurational space at progressively decreasing temperatures, following a simulated annealing protocol, were performed to identify adsorption configurations. The identified adsorbate–substrate configurations were ranked using our

previously described protocol [59, 60], and the lowest adsorption energy conformers were optimized with the Forcite module to obtain a stable conformation.

4. Results and discussion

4.1. Structural characterization of PdNP-BN

BN/CF and PdNP-BN/CF were successfully prepared by ALD. HR-TEM analysis of PdNP-BN/CF samples (**Fig. 2**A) indicated that PdNPs were well dispersed on the CF surface with a mean diameter of 6 nm (**Fig. 2**B). It also confirmed the deposition of a conformal and continuous ultrathin BN layer of ~2 nm on the CF surface (Fig. S1B-C). The number of ALD cycles to obtain the best BN thickness was studied, and was found to be 25 cycles. The Fast Fourier transform (FFT) spectra (**Fig. 2**C) confirmed the crystallinity of the deposited PdNPs. Energy-dispersive X-ray spectroscopy (EDS) maps of elements (**Fig. 2**D-F) confirmed the existence of B, N and Pd in the studied samples. The chemical state of C, B, N, O and Pd in modified CFs, evaluated by XPS, showed the presence of C, B, N, O and Pd in PdNP-BN/CF (**Fig. 2**G). The fitted B1s spectra displayed a peak centred at 192.5 eV (**Fig. 2**H) that was assigned to B−N bonding. In the N 1s spectra (**Fig. 2**I), the initial peak was divided in two major peaks that were assigned to N–O (398.2 eV) and B–N (400.1 eV). The Pd 3d3/2 and 3d5/2 binding energies were 340.9 and 335.6 eV, respectively (**Fig. 2**J). The deconvoluted peaks were assigned to Pd^0 and PdO_x, and the metal Pd^0 was a major phase. These results are similar to those previously published by Weber et al [61]. The presence of PdO_x species is related to the fact that BN attracts electrons from PdNPs. The O 1s and C 1s spectra are shown in Fig. S2.

Doping level is crucial because carrier density is crucial for fine-tuning the performance of the material. It has been established that doping Pd NPs with either electron-donating (nitrogen) or electron-withdrawing (boron) groups significantly alters the electrical properties of the NPs.

When the Pd NP is doped with electron-withdrawing (electron acceptors, p-type) or electron-donating (n-type, electron donors) groups, the electron density varies, which also influences the NP's electrochemical properties.

4.2. Characterization of the fabricated immunosensor (BSA/anti-AFB$_1$/L-Cys/PdNP-BN/CF)

AFM was used for the topographical and morphological analysis of the modified electrode because it is one of the most efficient techniques to evaluate the topographical and surface roughness. The 2D topographical AFM images of the L-Cys/PdNP-BN/CF electrode (Fig. S3A), obtained in static mode, showed the electrode surface topography after L-Cys modification. The surface layer was uniform and widespread without aggregates or layer faults, with a surface roughness (Rz) of 0.6028 µm. Upon immobilization of the anti-AFB$_1$ antibody on the L-Cys/PdNPs-BN/CF surface (Fig. S3B), the surface appeared more globular, indicating its protein nature [12]. The surface roughness increased to 1.2552 µm. This demonstrates that the homogeneity of the L-Cys layer allowed the uniform antibody binding to the functional moiety [62]. AFM revealed that this is an efficient approach to immobilize antibodies for immunosensor production. ATR spectroscopy was used to identify the functional groups at the immunosensor surface (**Fig. 2**K). The ATR spectra of PdNP-BN/CF (Fig. S4A) showed two bends at 825 cm^{-1} and 1572 cm^{-1} that are the B-N in plane stretching mode and the out of plane vibration of h-BN, respectively [63]. When the electrode was modified with L-Cys (**Fig. 2**K; curve i; L-Cys/PdNP-BN/CF), the spectrum showed four peaks. The peaks at 1446 cm^{-1} and 1365 cm-^{1} were assigned to the asymmetric and symmetric stretching of COO-, and those at 1528 cm^{-1} and 1299 cm^{-1} to the bending mode of –NH_2 and to the C-N bend, in agreement with the findings by Panhwar and co-workers [64]. The characteristic peak confirmed that L-Cys was modified on the electrode surface. A very weak thiol group (-SH) peak at 2585 cm^{-1} indicated that L-Cys was present on the electrode surface [65]. Antibody docking on L-

Cys/PdNP-BN (curve ii; anti-AFB_1/L-Cys/PdNP-BN/CF) resulted in peaks at 3001 cm^{-1}, 1689 cm^{-1}, and 866 cm^{-1} due to amide bond (N-H) deformation, stretching, and -NH_2, respectively, on the electrode surface [51, 66]. These data confirmed the antibody immobilization. After incubation with BSA (curve iii; BSA/anti-AFB_1/L-Cys/PdNP-BN/CF), the -NH_2 group disappearance from the spectrum confirmed that the non-specific sites on the anti-AFB_1/L-Cys/PdNPs-BN/CF immunosensor were blocked by BSA [67].

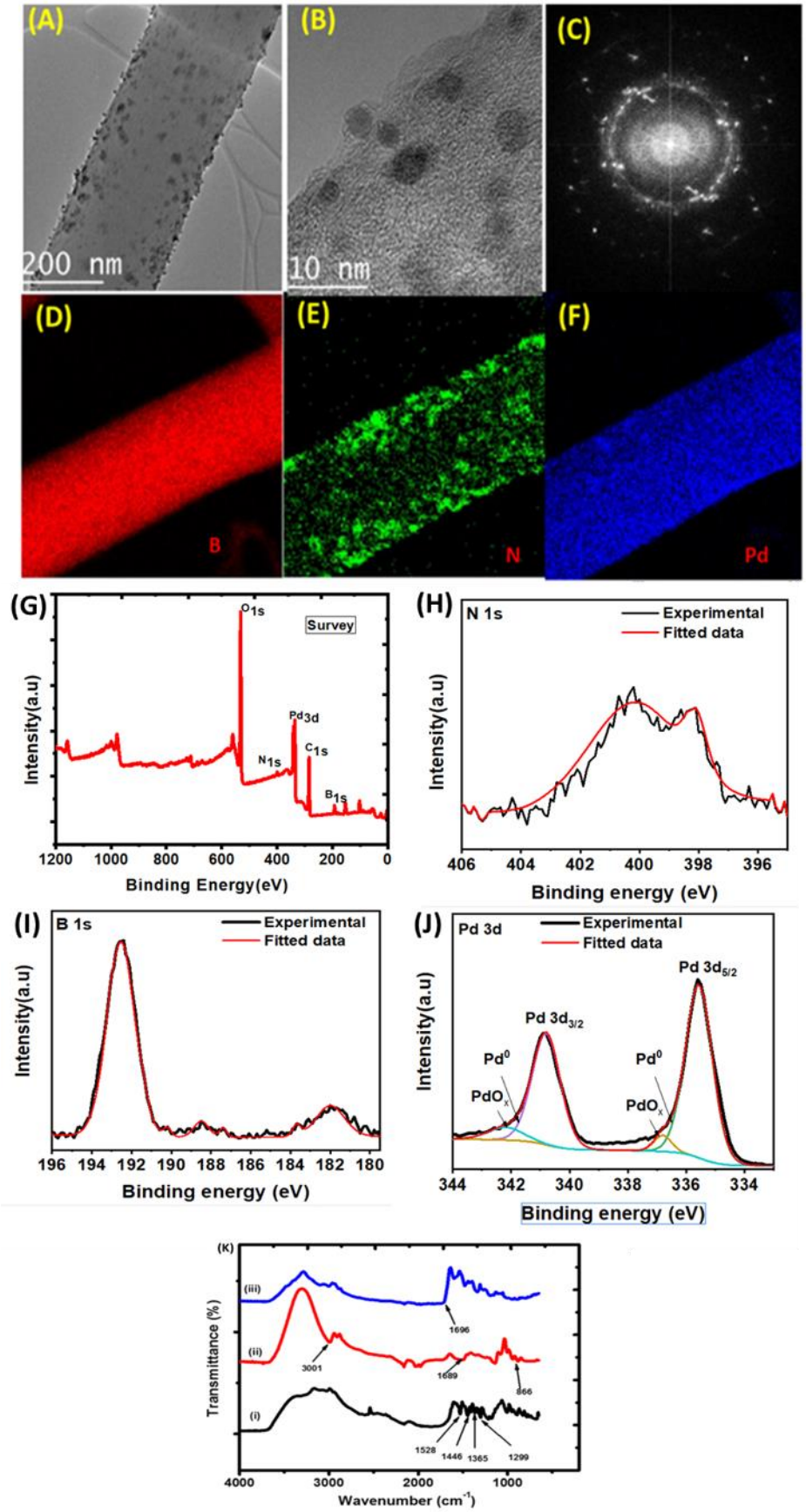

Fig. 2: (A-B) TEM micrographs of PdNP-BN at low and high magnification; (C) Fast Fourier transform spectrum of PdNP-BN; (D-F) EDS maps of B, N and Pd, respectively; same sample as in (A); (G) XPS survey spectrum of PdNP-BN/CF; (H-J) High-magnification XPS spectra

of B 1s, N 1s and Pd 3d, respectively; (K) ATR spectra of (i) L-Cys/PdNP-BN/CF, (ii) anti-AFB_1/L-Cys/PdNP-BN/CF, and (iii) BSA/anti-AFB_1/L-Cys/PdNP-BN/CF.

4.3. Electrochemical characterization of the electrode interfaces

CV and EIS in a 0.1M KCl and 5.0 mM $[Fe(CN)_6]^{3-/4-}$ (the redox probe) solution were used to characterize each step of the immunosensor fabrication process (**Fig. 3**A and B). For the PdNP-BN/CF sample (curve i), the electrochemical reaction was quasi-reversible with a peak separation at ~110 mV and 20 mV/s, and an anodic current (I_{pa}) of 1.45 µA. The current increase due to BN catalytic behaviour facilitated the electron transfer. L-Cys adsorption on the electrode surface led to a I_{pa} decrease to 0.73 µA (curve ii). L-Cys reduced the resistance of the electrostatic repulsion between the -COOH of L-Cys and $[Fe(CN)_6]^{3-/4-}$ negative charge [68]. Upon immobilization of the anti-AFB_1 antibodies to produce the anti-AFB_1/L-Cys/PdNP-BN/CF electrode, I_{pa} increased to 0.97 µA (curve iii). This indicates that the anti-AFB_1 antibodies act as a mediator activity between L-Cys/PdNP-BN and CF. The shorter electron tunnelling distance between antibodies and electrode explains the peak current increase [69]. Non-specific site blocking with BSA to form the BSA/anti-AFB_1/L-Cys/PdNP-BN/CF sensor resulted in a I_{pa} decrease to 0.50 µA (curve iv). This was caused by BSA adsorption on the surface. EIS is among the best tools to analyse the modified electrode surface [68]. The EIS shape includes high frequencies and low frequencies. The high frequencies contain a semicircle where electron transfers occur, whereas the low frequencies contain a linear portion where the electrochemical process occurs. The modified Randles circuit (inset in **Fig. 3**B) was used for fitting the impedance data. The circuit included the ohmic resistance of the electrolyte solution (Rs), double layer capacitance (Cdl), charge transfer resistance (Rct), and Warburg impedance element (Zw). Chen and co-workers showed that Rs and Zw are not affected by reactions taking place on the electrode surface. Conversely, Cdl and Rct are influenced by the insulating features and the electrode interface, respectively [70]. **Fig. 3**B shows the Nyquist plots for the

electrode at different modification steps. Rct and Zw were parallel with Cdl. The bare CF showed a small semicircle diameter with Rct = 9 Ω, implying a low charge transfer resistance (Fig. 4SB). In PdNPs-BN/CF (**Fig. 3**B; curve i), Rct slightly increased to 84 Ω, due to the excellent electrocatalytic activity of PdNPs and BN. When L-Cys was assembled onto the PdNP-BN/CF surface, Rct increased to 1200 Ω (curve ii). This shows that L-Cys formed a large barrier to the interfacial charge transfer, as indicated by the increasing semicircle diameter in the spectrum. Similar results were reported by Fan and co-workers [71]. When the anti-AFB1 antibody was covalently bound to L-Cys, Rct decreased to 567 Ω (curve iii), confirming the antibody immobilization on the surface of the modified electrode. Rct decreased also after BSA immobilization onto the modified electrode (curve iv), demonstrating the successful fabrication of the immunosensor.

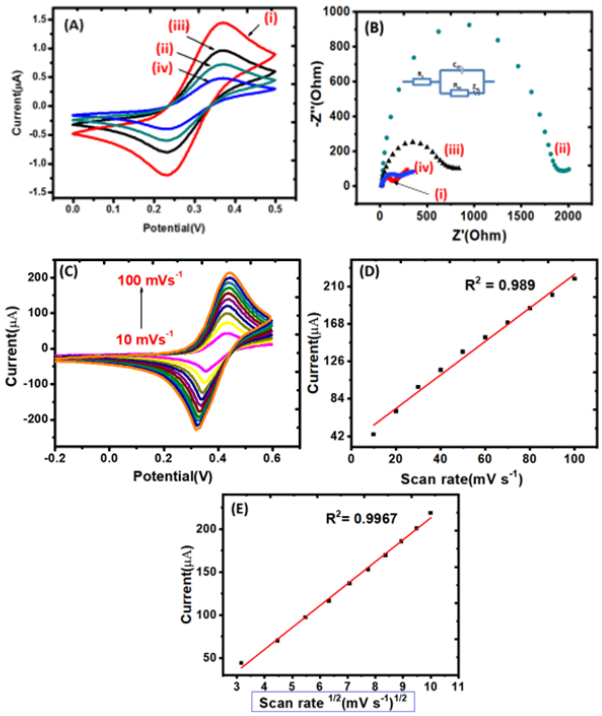

Fig. 3: (A) Cyclic voltammograms and (B) Nyquist plots for (i) PdNP-BN/CF, (ii) L-Cys/PdNP-BN/CF, (iii) anti-AFB_1/L-Cys/PdNP-BN/CF, and (iv) BSA/anti-AFB_1/L-Cys/PdNP-BN/CF. Conditions: solution of 0.1M PBS, 0.1M KCl and 5 mM $[Fe(CN)_6]^{3-/4-}$, pH 7.5, scan rate of 20 mV s^{-1}. (C) Relationship between peak current and scan rate. (D-E) Graphs

showing the relationship between cathodic peak current and scan rate (D) or the scan rate square root (E) for the BSA/anti-AFB_1/L-Cys/PdNP-BN/CF sensor in the same solution as for (A-B).

4.4. Investigation of the scan rate effects on BSA/anti-AFB_1/L-Cys/PdNP-BN/CF

To determine the electrochemical reaction mechanism of the developed immunosensor, the effect of different scan rates (ν) (from 10 to 100 mV s^{-1}) with BSA/anti-AFB1/L-Cys/PdNP-BN/CF was studied using CV (**Fig. 3**C). The linear increase of the current with the scan rate, in the redox probe, according to the equation I_{pa} (μA) = 1.882 ν (mV s^{-1}) + 35.689 (R^2 = 0.989), suggested a diffusion-controlled reaction (**Fig. 3**D). This was confirmed by the linear relationship between the scan rate square root and the cathodic current (**Fig. 3**E), in agreement with the observed diffusion-controlled reaction [72, 73].

4.5. Optimizing the experimental conditions

To improve the immunosensor analytical performance, key parameters (i.e. pH of the PBS solution, L-Cys concentration, incubation time for the specific binding to the target material, antibody concentration and immobilization time) were optimized using 6.0 ng mL^{-1} AFB_1. The pH effect was optimized by testing PBS solutions at different pH (from 5.5 to 8.5). The immunosensor peak current increased in the presence of PBS solutions up to pH = 7.5 and then decreased (**Fig. 4**A). This shows that a highly basic environment denatures the activity of the immobilized antibodies. Additionally, the Sigma-Aldrich safety data sheet indicates that the pH of the anti-AFB1 antibody is 7.4. This means that the antibody maintains its activity and stable combination with the antigen at neutral pH. Therefore, the PBS solution at pH 7.5 was chosen for AFB_1 detection. Then, various L-Cys concentrations (5.0, 10, 15, 20, and 25 mmol L^{-1}) were tested. The peak current increased when L-Cys concentrations from 5.0 to 10 mmol L^{-1} were used, and then decreased, due to electrode saturation (**Fig. 4**B). The incubation time role was the tested by varying the incubation time of the immunosensor (**Fig. 4**C). As the peak current progressively increased and reached a plateau at 30 min, this time duration was selected

as optimal. The concentration of antibodies immobilized on the electrode surface influences the sensor sensitivity due to the availability of more or fewer binding sites for antigens. Four different anti-AFB_1 antibody concentrations were tested (0.5, 1.0, 5.0 and 10 µg mL^{-1}) (**Fig. 4**D). The peak current increased when 0.5 to 1.0 µg mL^{-1} antibodies were immobilized, and then progressively decreased with increasing concentrations. Therefore, the anti-AFB_1 antibody concentration of 1.0 µg mL^{-1} was used for all experiments.

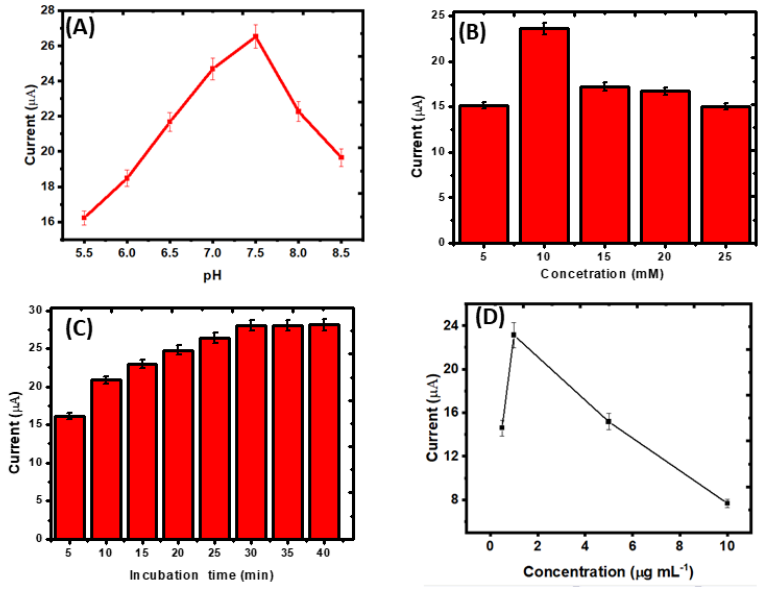

Fig. 4: Effects on the peak current of BSA/anti-AFB_1 /L-Cys/PdNP-BN/CF in the presence of 6 ng mL^{-1} AFB_1 of the following parameters (A) pH, (B) L-Cys concentration, (C) incubation time, and (D) anti-AFB_1 antibody concentration. The electrochemical experiments were performed in a solution of 0.1M KCl, 0.1M PBS (pH 7.4) and 5 mM $[Fe(CN)_6]^{3-/4-}$.

4.6. Sensing mechanisms of the immunosensor

In this work, the immunosensor was fabricated by immobilizing L-Cys on the PdNP-BN/CF electrode surface to form thiolated bonds. The PdNP-BN surface was used as a carrier of the electrochemical capture probe to increase the peak current change. Then, the terminal carboxylic groups present in the thiolated bond were converted to NHS esters by attaching the crosslinker (EDC:NHS) to L-Cys/PdNP-BN/CF. The anti-AFB_1 antibody was then covalently attached to the NHS esters, followed by incubation with BSA to block the immunosensor non-

specific sites. The ferricyanide solution was used as redox mediator to generate the electron flow between the bulk solution and the working electrode. In the absence of AFB_1, the anti-AFB_1 antibodies gave a significantly strong faradaic current. Conversely, in the presence of AFB_1, the faradaic current decreased because the formation of anti-AFB_1 antibody-AFB_1 complexes hinders the electron transfer of $Fe(CN)_6^{3-}/Fe(CN)_6^{4-}$ [74, 75].

4.7. Analytical characteristics of the BSA/anti-AFB_1/L-Cys/PdNP-BN/CF immunosensor

The performance of the fabricated immunosensor was verified using AFB_1 at different concentrations (1.0 to 10 ng mL^{-1}) and the optimized parameters. The LSV curves (from triplicate measurements) showed that the peak current decreased with higher AFB_1 concentrations (**Fig. 5**A). This is due to hindrance of electron transfer to the electrode after AFB_1 adsorption onto the BSA/anti-AFB_1/L-Cys/PdNP-BN/CF immunosensor. Specifically, at the tested concentrations, the peak current displayed a linear relationship with AFB_1 detection (R^2 = 0.9987), and the limit of detection (LOD) was 0.834 ng mL^{-1} (3×se)/m) (**Fig. 5**B). These results are in agreement with the reference range and indicate that the immunosensor can be used to detect AFB_1 in alcoholic beverages. The immunosensor precision was determined by consecutive determination of 6.0 ng mL^{-1} of AFB_1 for 20 times using the same experimental set-up and immunosensor. This experiment gave a relative standard deviation (RSD) of 1.5%. Reproducibility was assessed using six different electrodes fabricated independently and gave an RSD of 1.2%. These results demonstrate that the fabricated immunosensor possesses good reproducibility and tolerable precision (Fig. S6A). Moreover, after storage in an airtight container at 4 °C for 3 weeks, the immunosensor peak current was 81.74% of the initial value, indicating good stability (Fig. S6B). The specificity of label-free immunosensors generally is limited, possibly due to non-specific adsorption of foreign compounds on the sensing surface. Therefore, the detection by the immunosensor of OTA and AFB_1 (1 ng mL^{-1} and 10 ng mL^{-1}) individually and mixed was evaluated. A negligible peak

current was observed when the immunosensor was incubated with OTA or the mixture, even at the higher concentration. Conversely, the peak current noticeably changed in the presence of AFB_1. These results show that the fabricated immunosensor is specific for AFB_1 (Fig. S6C). Compared with other electrochemical immunosensors for AFB_1 detection (Table S1), the fabricated immunosensor had a low detection limit and acceptable detection range. Its good electrochemical performance could be explained by the wide surface area, good bio-compatibility, and good signal electrochemical amplification of the L-Cys/PdNP-BN composite. In addition, the large anti-AFB_1 antibody amount loaded onto the L-Cys/PdNP-BN surface enhances the possibility of antigen binding.

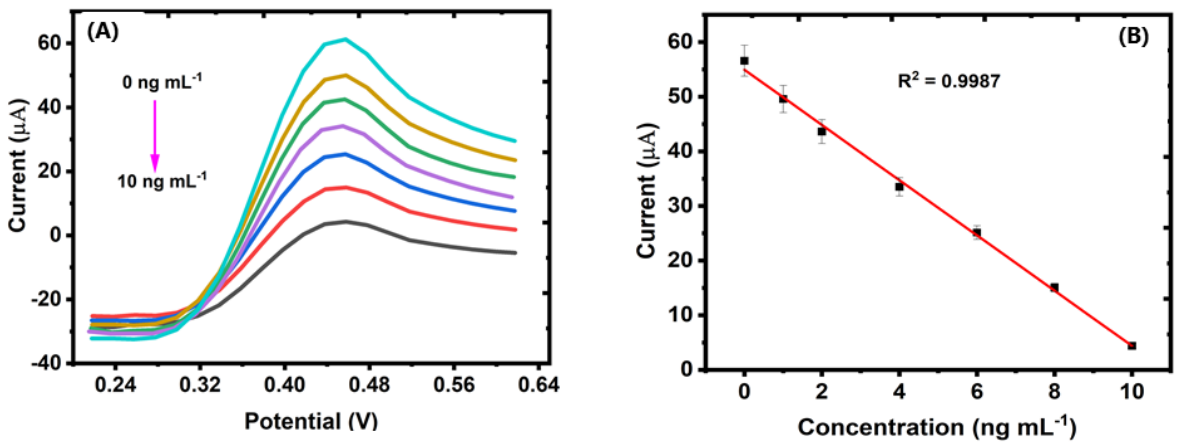

Fig. 5: (A) LSV curves for BSA/anti-AFB_1/L-Cys/PdNP-BN/CF when using different AFB_1 concentrations (0.0, 1.0, 2.0, 4.0, 6.0, 8.0, 10.0 ng mL^{-1}), and (B) Linear calibration curve of AFB_1 concentrations.

4.8. Recovery studies

The fabricated immunosensor capacity to identify AFB_1 in wine samples was then investigated by spiking wine samples with various AFB_1 concentrations chosen on the basis of the AFB_1 calibration curve (**Fig. 5**B). The fabricated immunosensor recovery levels varied between 93.00% and 106.00%, and the proportional error ranged from 1.83 to 6.0% (**Table 1**). These data indicate that the fabricated immunosensor can be used to detect AFB_1 in wine.

Table 1: Quantitative determination of AFB_1 in wine samples.

AFB_1 added (ng mL^{-1})	**AFB_1 detected (ng mL^{-1})**	**Recovery (%)**	**Proportional error (%)**
2.0	2.12	106.00	6.0
4.0	3.89	97.75	2.75
6.0	5.89	98.17	1.83
8.0	8.34	93.00	4.25

4.9. Computational modelling

4.9.1. Molecular docking

Molecular docking studies were performed to investigate the preferred binding sites of the BSA-anti-AFB_1 antibody substrate. **Fig. 6** shows the best docked pose and binding site of the substrate. The best binding site (site 1) was located in the hydrophobic cavity of BSA, known as subdomain IIA [76].

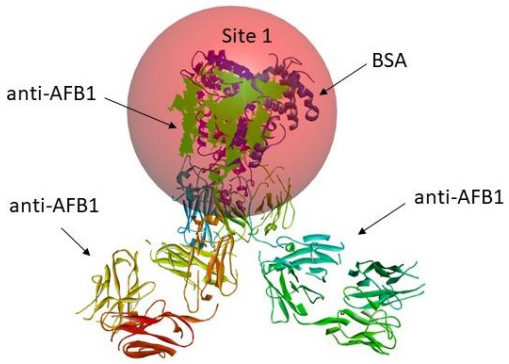

Fig. 6: Best docked pose and binding site for the BSA-anti-AFB_1 antibody complex.

4.9.2. Monte Carlo adsorption simulations

Monte Carlo adsorption simulations were preformed to investigate the substrate-adsorbate interaction energetics and to validate the experimental (CV) results of the BSA/anti-AFB_1/L-Cys/PdNP-BN/CF immunosensor.

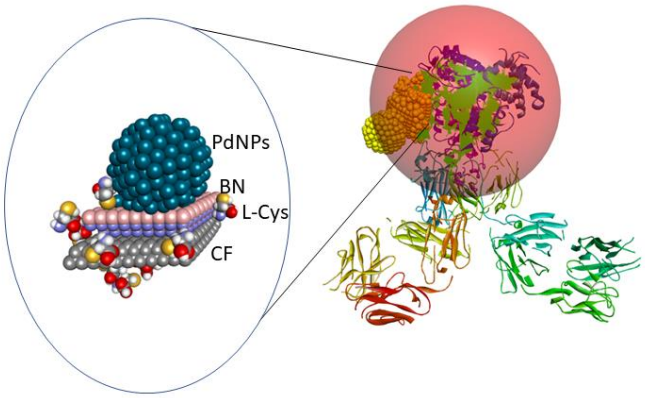

Fig. 7: Lowest energy configuration of the BSA/anti-AFB_1/L-Cys/PdNP-BN/CF immunosensor using Monte Carlo simulations.

The calculated adsorption energy for the immunosensor (**Fig. 7**) was strongly negative, indicating stabilization and an exothermic adsorption process [55, 57], implying stronger adsorption energy. This result explains why non-specific site blocking with BSA to form BSA-anti-AFB_1/L-Cys/PdNP-BN/CF resulted in a I_{pa} decrease to 0.50 µA (**Fig. 3**A, iv). The major forces that stabilized the complex were hydrogen bonding and van der Waals interactions.

Our modelling results (see supplementary information) also showed that the adsorption energies increased from the PdNP-BN/CF to the L-Cys/PdNP-BN/CF nanocomposite, suggesting higher stabilization due to the strong interaction of L-Cys with the electrode surface, in line with the amplified electrochemical signals in **Fig. 3**A **(i-ii)**. This also supports the catalytic behaviour of BN that facilitates electron transfer.

5. Conclusion

The anti-AFB_1 antibody was immobilized onto the L-Cys- and PdNP-functionalized BN/CF electrode for AFB_1 detection. The fabricated immunosensor displayed adequate reproducibility and high specificity and sensitivity for AFB_1 detection in wine samples, from 1.0 to 10 ng mL^{-1} (LOD of 0.832 ng mL^{-1}). Our results demonstrated the multifunctional nanocomposite synergistic effects. Specifically, in the presence of EDC/NHS activation, L-Cys provided electron activity due to its electrochemical property, PdNPs offered sites for the antibody covalent immobilization, and BN gave good electric conductivity and rigidity to increase stability. Moreover, computational modelling was used to complement and validate the experimental data. The developed method offers a universal strategy for AFB_1 detection in wine, and could pave the way to the development of a sensitive device for wine safety and screening applications.

Declaration of Competing Interest

The authors state that they do not have any conflict of interest.

Acknowledgments

We thank the French Embassy Scholarship from South Africa and the Council for Scientific and Industrial Research (CSIR) for their financial support. KB thanks the Centre for High Performance Computing, Cape Town, South Africa, for computational resources. We also express our deep appreciation to Michel Ramonda for his help with AFM studies. I acknowledges the financial support by RISE-H2020-EU.1.3.3. Grant (ID: 778157) CanBioSe and the Polish National Science Centre (NCN) for the OPUS grant 2020/37/B/ST5/00576.

6. References

[1] H.J.V.d. Fels-Klerx, C. Liu, P. Battilani, Modelling climate change impacts on mycotoxins contamination, *World Mycotoxin J.* 9(5) (2016) 717-726

[2] A. Beheshti-Marnani, A. Hatefi-Mehrjardi, Z. Es'haghi, A sensitive biosensing method for detecting of ultra-trace amounts of AFB1 based on "Aptamer/reduced graphene oxide" nano-bio interaction, *Colloids Surf. B: Biointerfaces* 175 (2019) 98-105

[3] K. Abnous, N.M. Danesh, M. Alibolandi, M. Ramezani, A.S. Emrani, R. Zolfaghari, S.M. Taghdisi, A new amplified π-shape electrochemical aptasensor for ultrasensitive detection of aflatoxin B_1, *Biosens. Bioelectron* 94 (2017) 374-379

[4] M. Joo, S.H. Baek, S.A. Cheon, H.S. Chun, S.-W. Choi, T.J. Park, Development of aflatoxin B1aptasensor based on wide-rangefluorescence detection using graphene oxide quencher, *Colloids Surf. B: Biointerfaces* 154 (2017) 27-32

[5] X. Guo, F. Wen, N. Zheng, Q. Luo, H. Wang, H. Wang, S. Li, J. Wang, Developmentofanultrasensitiveaptasensorforthedetection of aflatoxin B_1, *Biosens. Bioelectron.* 56 (2014) 340-344

[6] K.Y. Goud, A. Hayat, G. Catanante, S. M., K.V. Gobi, J.L. Marty, An electrochemical aptasensor based on functionalized graphene oxideassisted electrocatalytic signal amplification of methylene blue for aflatoxin B_1 detection, *Electrochim. Acta* 244 (2017) 96-103

[7] S.S. Wu, M. Wei, W. Wei, Y. Liu, S. Liu, Electrochemical aptasensor for aflatoxin B1 based on smart host-guest recognition of β-cyclodextrin polymer, *Biosens. Bioelectron.* 19 (20019) 58-63

[8] G. Evtugyn, A. Porfireva, V. Stepanova, R. Sitdikov, I. Stoikov, D. Nikolelis, T. Hianik, Electrochemical Aptasensor Based on PolycarboxylicMacrocycle Modified with Neutral Red for Aflatoxin B_1 Detection, *Electroanalysis* 26 (2014) 2100 – 2109

[9] K.Y. Goud, G. Catanante, A. Hayat, S. M., K.V. Gobi, J.L. Marty, Disposable and portable electrochemical aptasensor for label free detection of aflatoxin B_1 in alcoholic beverages, *Sens. Actuators B Chem.* 235 (2016) 466-473

[10] G.S. Geleta, Z. Zhao, Z. Wang, Novel reduced graphene oxide/molybdenum disulfide/polyaniline nanocomposite based electrochemical aptasensor for detection of aflatoxin B_1, *Analyst* 143(7) (2018) 1644-1649

[11] C. Wang, J. Qian, K. An, X. Huang, L. Zhao, Q. Liu, Nan Hao, K. Wang, Magneto-controlled aptasensor for simultaneous electrochemical detection of dual mycotoxins in maize using metal sulfide quantum dots coated silica as labels, *Biosens. Bioelectron.* 89 (20017) 802-809

[12] E.P. Simão, G.J.L.S. Barbieri, C.A.S. Andrade, M.D.L. Oliveira, Biosensor Based on Cysteine Monolayer and Monoclonal Antibody for Specific Detection of Aflatoxin B_1 in Rice, *J. Braz. Chem. Soc* 27(6) (2016) 1040-1047

[13] W. Zheng, J. Teng, L. Cheng, Y. Ye, D. Pan, J. Ye, F. Xue, G. Liu, W. Chen, Hetero-enzyme-based two-round signal amplification strategy for trace detection of aflatoxin B1 using an electrochemical aptasensor, *Biosens. Bioelectron.* 80 (2016) 574-581

[14] M.F. Adallah, G. Girgin, T. Baydar, R. Krska, M. Sulyok, Occurrence of multiple mycotoxins and other fungal metabolites in animal feed and maize samples from Egypt using LC-MS/MS, *J. Sci. Food Agric.* 97(13) (2017) 4419-4428

[15] Y. Xiong, K. Pei, Y. Wu, H. Duan, W. Lai, Y. Xiong, Plasmonic ELISA based on enzyme-assisted etching of Au nanorods for the highly sensitive detection of aflatoxin B1 in corn samples, *Sens. Actuators B Chem.* 276 (2018) 320-327

[16] L.-L. Qu, Q. Jia, C. Liu, W. Wang, L. Duan, G. Yang, C.-Q. Han, H. Li, Thin layer chromatography combined with surface-enhanced raman spectroscopy for rapid sensing aflatoxins, *J. Chromatogr. A* 1579 (2018) 115-120

[17] S.S. Saini, M. Adel-Rehim, Integrated extraction approach for trace analysis of aflatoxin B1 in domestic water tanks using HPLC, *Sep. Sci. Plus* 3(5) (2020) 167-174

[18] V. Myndrul, R. Viter, M. Savchuk, M. Koval, N. Starodub, V. Silamiķelis, V. Smyntyna, A. Ramanavicius, I. Iatsunskyi, Gold coated porous silicon nanocomposite as a substrate for photoluminescence-based immunosensor suitable for the determination of Aflatoxin B1, *Talanta* 175 (2017) 297-304
[19] V. Myndrul, E. Coy, M. Bechelany, I. Iatsunskyi, Photoluminescence label-free immunosensor for the detection of Aflatoxin B1 using polyacrylonitrile/zinc oxide nanofibers, *Mater. Sci. Eng. C* 118 (2021) 111401
[20] M. Jiang, M. Braiek, A. Florea, A. Chrouda, C. Farre, A. Bonhomme, F. Bessueille, F. Vocanson, A. Zhang, N.J.T. Jaffrezic-Renault, Aflatoxin B1 detection using a highly-sensitive molecularly-imprinted electrochemical sensor based on an electropolymerized metal organic framework, *Toxins (Basel)* 7(9) (2015) 3540-3553
[21] J. Ge, Y. Zhao, C. Li, G.J.A.c. Jie, Versatile electrochemiluminescence and electrochemical "on–off" assays of methyltransferases and aflatoxin b1 based on a novel multifunctional DNA nanotube, *Anal. Chem.* 91(5) (2019) 3546-3554
[22] Y. Lu, B. Zhang, Y. Tian, Q. Guo, X. Yang, G.J.M.A. Nie, An enhanced photoelectrochemical sensor for aflatoxin B1 detection based on organic-inorganic heterojunction nanomaterial: poly (5-formylindole)/NiO, *Microchim. Acta* 187(8) (2020) 1-9
[23] F.A. Azri, R. Sukor, J. Selamat, F. Abu Bakar, N.A. Yusof, R.J.T. Hajian, Electrochemical immunosensor for detection of aflatoxin B1 based on indirect competitive ELISA, *Toxins (Basel).* 10(5) (2018) 196
[24] I. Saldan, Y. Semenyuk, I. Marchuk, O.J.J.o.M.S. Reshetnyak, Chemical synthesis and application of palladium nanoparticles, *J. Mater. Sci.* 50(6) (2015) 2337-2354
[25] V. Leso, I.J.I.j.o.m.s. Iavicoli, Palladium nanoparticles: toxicological effects and potential implications for occupational risk assessment, *Int J Mol Sci.* 19(2) (2018) 503
[26] T. Yan, L. Zhu, H. Ju, J.J.A.c. Lei, DNA-Walker-Induced allosteric switch for tandem signal amplification with palladium nanoparticles/metal–organic framework tags in electrochemical biosensing, *Anal. Chem.* 90(24) (2018) 14493-14499
[27] X. Yi, Y. Wu, G. Tan, P. Yu, L. Zhou, Z. Zhou, J. Chen, Z. Wang, J. Pang, C.J.S.r. Ning, Palladium nanoparticles entrapped in a self-supporting nanoporous gold wire as sensitive dopamine biosensor, *Sci. Rep.* 7(1) (2017) 1-9
[28] C.T.J.S.s.r. Campbell, Ultrathin metal films and particles on oxide surfaces: structural, electronic and chemisorptive properties, *Surf. Sci. Rep.* 27(1-3) (1997) 1-111
[29] M. Weber, J.-Y. Kim, J.-H. Lee, J.-H. Kim, I. Iatsunskyi, E. Coy, P. Miele, M. Bechelany, S.S.J.J.o.M.C.A. Kim, Highly efficient hydrogen sensors based on Pd nanoparticles supported on boron nitride coated ZnO nanowires, *J. Mater. Chem. A* 7(14) (2019) 8107-8116
[30] D. Kong, H. Wang, Z. Lu, Y.J.J.o.t.A.C.S. Cui, CoSe2 nanoparticles grown on carbon fiber paper: an efficient and stable electrocatalyst for hydrogen evolution reaction, *J. Am. Chem. Soc.* 136(13) (2014) 4897-4900
[31] M. Weber, J.-Y. Kim, J.-H. Lee, J.-H. Kim, I. Iatsunskyi, E. Coy, P. Miele, M. Bechelany, S.S. Kim, Highy effient hydrogen sensors based on Pd nanoparticles supported on boron nitride coated ZnO nanowires, *J. Mater. Chem. B* 7(14) (2019) 8107-8116
[32] M. Weber, C. Lamboux, B. Navarra, P. Miele, S. Zanna, M.E. Dufond, L. Santinacci, M.J.N. Bechelany, Boron nitride as a novel support for highly stable palladium nanocatalysts by atomic layer deposition, *Nanomaterials (Basel)* 8(10) (2018) 849
[33] S. Yu, X. Wang, H. Pang, R. Zhang, W. Song, D. Fu, T. Hayat, X. Wang, Boron nitride-based materials for the removal of pollutants from aqueous solution: a review, *Chem. Eng. J.* 333 (2018) 343-360
[34] S. Angizi, M. Khalaj, S.A.A. Alem, A. Alem, A. Pakdel, M. Willander, A. Hatamie, A. Simchi, Towards the Two-Dimensional Hexagonal Boron Nitride (2D-h-BN) Electrochemical Sensing Platforms, *J. Electrochem. Soc.* 167(12) (2020) 126513

[35] A. Harley-Trochimczyk, T. Pham, J. Chang, E. Chen, M. A.Worsley, A. Zettl, W. Mickelson, R. Maboudian, Platinum Nanoparticles Loading of Boron Nitride Aerogel and Its Use as a Novel Material for Low-Power Catalytic Gas Sensing, *Adv. Funct. Mater.* 26(3) (2016) 433-439
[36] H. Li, Y. He, T. He, D. Qing, F. Luo, Y. Fan, X. Chen, Ni-W/BN(h) electrodeposited nanocomposite coating with functionally graded microstructure, *J. Alloys Compd.* 704 (2017) 32-43
[37] C. Zhang, Y. He, F. Li, H. Di, L. Zhang, Y. Zhan, h-BN decorated with Fe_3O_4 nanoparticles through mussel-inspired chemistry of dopamine for reinforcing anticorrosion perfomance of epoxy coatings, *J. Alloys Compd.* 685 (2016) 743-751
[38] K.L. Firestein, D.V. Leybo, A.E. Steinman, A.M. Kovalskii, A.T. Matveev, A.M. Manakhov, I.V. Sukhorukova, P.V. Slukin, N.K. Fursova, S.G. Ignatov, D.V. Golberg, D.V. Shtansky, BN/Ag hybrid nanomaterials with petal-like surfaces as catalysts and antibacterial agents, *Beilstein J. Nanotechnol.* 9(1) (2018) 250-261
[39] W. Han, Z. Ma, S. Liu, C. Ge, L. Wang, X. Zhang, Highy-dispersible boron nitride nanoparticles by spray drying and pyrolysis, *Ceram. Int.* 43(13) (2017) 10192-10200
[40] P.O. Oviroh, R. Akbarzadeh, D. Pan, R.A.M. Coetzee, T.-C. Jen, New development of atomic layer deposition: processes, methods and applications, *Sci Technol Adv Mater.* 20(1) (2019) 465-496
[41] O. Graniel, M. Weber, S. Balme, P. Miele, M. Bechelany, Atomic layer deposition for biosensing applications, *Biosens. Bioelectron.* 122 (2018) 147-159
[42] M. Weber, A. Julbe, A. Ayral, P. Miele, M. Bechelany, Atomic layer deposition for membranes: Basics,Challenges , and Opportunities, *Chem. Mater.* 30(21) (2018) 7368-7390
[43] Z. Zhang, Y. Zhang, H. Yu, S. Rong, H. Gao, L. Meng, J. Dai, H. Pan, D. Chang, Spherical carrier amplification strategy for electrochemical immunosensor based on polystyrene-gold nanorods @L-cysteine/MoS_2 for determination of tacrolimus, *Talanta* 220 (2020) 121321
[44] Y. Kawano, M. Shiroyama, K. Kanazawa, Y.A. Suzuki, I. Ohtsu, Development of high-throughput quantitative analytical method for l-cysteine-containing dipeptides by LC–MS/MS toward its fermentative production, *AMB Express* 9(1) (2019) 1-9
[45] S.-I. Oh, J.-K. Park, S.-K. Park, Lifespan extension and increased resistance to environmental stressors by N-acetyl-L-cysteine in Caenorhabditis elegans, *Clinics* 70(5) (2015) 380-386
[46] F. Bamdad, F. Khorram, M. Samet, K. Bamdad, M.R. Sangi, F.J.S.A.P.A.M. Allahbakhshi, B. Spectroscopy, Spectrophotometric determination of L-cysteine by using polyvinylpyrrolidone-stabilized silver nanoparticles in the presence of barium ions, *Spectrochim. Acta A Mol.* 161 (2016) 52-57
[47] N. Kumar, L.S.B.J.A.S.S. Upadhyay, Facile and green synthesis of highly stable l-cysteine functionalized copper nanoparticles, *Appl. Surf. Sci.* 385 (2016) 225-233
[48] P. Mulpur, A. Kurdekar, R. Podila, A.M. Rao, V.J.N.R. Kamisetti, Surface plasmon coupled emission as a novel analytical platform for the sensitive detection of cysteine, *Nanotechnol. Rev.* 4(5) (2015) 393-400
[49] A. Asfaram, M. Ghaedi, S. Agarwal, I. Tyagi, V.K.J.R.a. Gupta, Removal of basic dye Auramine-O by ZnS: Cu nanoparticles loaded on activated carbon: optimization of parameters using response surface methodology with central composite design, *RSC Adv.* 5(24) (2015) 18438-18450
[50] B.R. Khalkho, R. Kurrey, M.K. Deb, K. Shrivas, S.S. Thakur, S. Pervez, V.K.J.H. Jain, L-cysteine modified silver nanoparticles for selective and sensitive colorimetric detection of vitamin B1 in food and water samples, *Heliyon* 6(2) (2020) e03423
[51] K. Kunene, M. Weber, M. Sabela, D. Voiry, S. Kanchi, K. Bisetty, M. Bechelany, Highly-efficient electrochemical label-free immunosensor for the detection of ochratoxin A in coffee samples, *Sens. Actuators B Chem.* 305 (2020) 127438
[52] W.E. Kosimaningrum, T.X.H. Le, Y. Holade, M. Bechelany, S. Tingry, B. Buchari, I. Noviandri, C. Innocent, M. Cretin, Surfactant-and binder-free hierarchical platinum nanoarray directly grown onto a carbon felt electrode for efficient electrocatalysis, *ACS Appl. Mater. Interfaces.* 9(27) (2017) 22476-22489

[53] M. Weber, N. Tuleushova, J. Zgheib, C. Lamboux, I. Iatsunskyi, E. Coy, V. Flaud, S. Tingry, D. Cornu, P. Miele, M. Bechelany, Y. Holade, Enhanced electrocatalyctic perfomance triggered by atomically bridged boron nitride between palladium nanoparticles and carbon fibers in gas-diffusion electrodes, *Appl. Catal.* 257 (2019) 117917
[54] L.T. Tran, T.Q. Tran, H.P. Ho, X.T. Chu, T.A. Mai, Simple label-free electrochemical immunosensor in a microchamber for detecting newcastle disease virus, *J. Nanomater.* 2019 (2019)
[55] L.J. Harris, S.B. Larson, K.W. Hasel, A. McPherson, Refined structure of an intact IgG2a monoclonal antibody, *Biochemistry* 36(7) (1997) 1581-1597
[56] K.A. Majorek, P.J. Porebski, A. Dayal, M.D. Zimmerman, K. Jablonska, A.J. Stewart, M. Chruszcz, W. Minor, Structural and immunologic characterization of bovine, horse, and rabbit serum albumins, *Mol. Immunol.* 52(3-4) (2012) 174-182
[57] R. Brenke, D.R. Hall, G.-Y. Chuang, S.R. Comeau, T. Bohnuud, D. Beglov, O. Schueler-Furman, S. Vajda, D. Kozakov, Application of asymmetric statistical potentials to antibody–protein docking, *Bioinformatics* 28(20) (2012) 2608-2614
[58] J. Ulicny, T. Kozar, Roadmap for Computer-Aided Modeling of Theranostics and Related Nanosystems, EPJ Web Conf., EDP Sciences, 2018, p. 05017.
[59] L. Naidoo, K. Suvardhan, M.I. Sabela, K. Bisetty, Multivariate optimization of field-flow fractionation of nanoscale synthetic amorphous silica in processed foods supported by computational modelling, *New J. Chem.* 44(40) (2020) 17542-17551
[60] A. Bathinapatla, S. Kanchi, M.I. Sabela, Y.C. Ling, K. Bisetty, Experimental and Computational Studies of a Laccase Immobilized ZnONPs/GO-Based Electrochemical Enzymatic Biosensor for the Detection of Sucralose in Food Samples, *Food Anal. Methods* 13(11) (2020) 2014-2027
[61] M. Weber, N. Tuleushova, J. Zgheib, C. Lamboux, I. Iatsunskyi, E. Coy, V. Flaud, S. Tingry, D. Cornu, P. Miele, M. Bechelany, Y. Holade, Enhanced electrocatalytic perfomanve triggered by atomically bridged boron nitride between palladium nanoparticles and caron fibers in gas-diffusion electrodes, *Appl. Catal.* 257 (2019) 117917-
[62] Q. Xue, C. Bian, J. Tong, J. Sun, H. Zhang, S. Xia, FET immunosensor for hemoglobon A1c using a gold nanofilm grown by a seed-mediated technique and covered with mixed sekf-assembled monolayers, *Microchim. Acta* 176(1-2) (2012) 65-72
[63] E. Dogan, Hydrogen production and its storage from solar energy, *Adv. Mater. Sci.* 20(2) (2020) 14-25
[64] S. Panhwar, S.S. Hassan, R.B. Mahar, A. Canlier, S. Uddin, M. Arain, Synthesis of l-Cysteine Capped Silver Nanoparticles in Acidic Media at Room Temperature and Detailed Characterization, *J. Inorg. Organomet. Polym. Mater.* 28(3) (2018) 863-870
[65] K.B.A. Ahmed, M. Sengan, S.K. P, A. Veerappan, Highy selective colorimetric cysteine sensor based on the fotmation of cysteine layer on copper nanoparticles, *Sens. Actuators B Chem.* 233 (2016) 431-437
[66] S. Lou, J.-y. Ye, K.-q. Li, A. Wu, A Gold nanoparticles-based immunochromatogaphic assay: The infuance of nano[article size, *Analyst* 137(5) (2011) 1174
[67] P.R. Solanki, M.K. Patel, M.A. Ali, B. Malhotra, A chitosan modified nickel oxide plaform for biosensing applications, *J. Mater. Chem. B* 3(32) (2015) 6698-6708
[68] P. Hashemi, A. Afkhami, H. Bagheri, S. Amidi, T. Madrakian, Fabrication of a novel impedimetric sensor based on L-Cysteine/Cu(II) modified gold electrode for sensitive determination of ampyra, *Anal. Chim. Acta* 984 (2017) 185-192
[69] S. Tiwari, P.K. Gupta, Y. Bagbi, T. Sarkar, P.R. Solanki, L-cysteine capped lanthanum hydroxie nanostructures for non-invasive detection of oral cancer biomarker, *Biosens. Bioelectron.* 89 (2017) 1042-1052
[70] L. Chen, J. Jiang, G. Shen, R. Yu, A label-free electrochemical impedance immunosensor for the sensitive detection of aflatoxin B_1, *Anal. Methods.* 7(6) (2015) 2354-2359

[71] A. Fan, L. Shi, H. Yang, G. Yang, A Novel Electrochemical Impedance Immunosensor for Aflatoxin B1 Based on L-cysteine Self-Assesmbled on Au Nanoparticles-Porous Nitrogen Doped Graphene Modified Electrode, *Int. J. Electrochem. Sci* 15 (2020) 9669-9682
[72] A. Dettlaff, P. Jakobczyk, M. Ficek, B. Wilk, M. Szala, J. Wojtas, T. Ossowski, R. Bogdanowicz, Electrochemical determination of nitroaromatic explosives at boron-doped diamond/graphene nanowall electrodes:2, 4 ,6-trinotrotoluene and 2, 4, 6-trinitroanisole in liquid effluents, *J. Hazard. Mater.* 387 (2020) 121672
[73] P.B. Deroco, I.G. Melo, L.S. Silva, K.I. Eguiluz, G.R. Salazar-Banda, O. Fatibello-Filho, Carbon black supported Au-Pd core-shell nanoparticles within a dihexadecylphosphate film for the development of hydrazine electrochemical sensor, *Sens. Actuators B Chem.* 256 (2018) 535-542
[74] Y.S. Kim, J.H. Niazi, M.B. Gu, Specific detection of oxytetracycline using DNA aptamer-immobilized interdigitated array electrode chip, *Anal. Chim. Acta* 634(2) (2009) 250-254
[75] L. Zhou, D.-J. Li, L. Gai, J.-P. Wang, Y.-B. Li, Electrochemical aptasensor for the detection of tetracycline with multi-walled carbon nanotubes amplification, *Sens. Actuators B Chem.* 162(1) (2012) 201-208
[76] S.K. Chaturvedi, E. Ahmad, J.M. Khan, P. Alam, M. Ishtikhar, R.H. Khan, Elucidating the interaction of limonene with bovine serum albumin: a multi-technique approach, *Mol. Biosyst.* 11(1) (2015) 307-316